Effective field theory in the harmonic oscillator basis

S. Binder, A. Ekström, G. Hagen, T. Papenbrock, and K. A. Wendt

Phys. Rev. C **93**, 044332 — Published 25 April 2016

DOI: 10.1103/PhysRevC.93.044332

Effective field theory in the harmonic oscillator basis

S. Binder,[1,2] A. Ekström,[1,2] G. Hagen,[2,1] T. Papenbrock,[1,2] and K. A. Wendt[1,2]

[1] *Department of Physics and Astronomy, University of Tennessee, Knoxville, TN 37996, USA*
[2] *Physics Division, Oak Ridge National Laboratory, Oak Ridge, TN 37831, USA*

We develop interactions from chiral effective field theory (EFT) that are tailored to the harmonic oscillator basis. As a consequence, ultraviolet convergence with respect to the model space is implemented by construction and infrared convergence can be achieved by enlarging the model space for the kinetic energy. In oscillator EFT, matrix elements of EFTs formulated for continuous momenta are evaluated at the discrete momenta that stem from the diagonalization of the kinetic energy in the finite oscillator space. By fitting to realistic phase shifts and deuteron data we construct an effective interaction from chiral EFT at next-to-leading order. Many-body coupled-cluster calculations of nuclei up to ^{132}Sn converge fast for the ground-state energies and radii in feasible model spaces.

PACS numbers: 21.30.-x, 21.30.Fe, 21.10.Dr, 21.60.-n

I. INTRODUCTION

The harmonic oscillator basis is advantageous in nuclear-structure theory because it retains all symmetries of the atomic nucleus and provides an approximate mean-field related to the nuclear shell model. However, interactions from chiral effective field theory (EFT) [1, 2] are typically formulated in momentum space, while the oscillator basis treats momenta and coordinates on an equal footing, thereby mixing long- and short-ranged physics. This incommensurability between the two bases is not only of academic concern but also makes oscillator-based *ab initio* calculations numerically expensive. Indeed, the oscillator basis must be large enough to accommodate the nucleus in position space as well as to contain the high-momentum contributions of the employed interaction. Furthermore, one needs to perform computations at different values of the oscillator spacing $\hbar\omega$ to gauge model-space independence of the computed results [3–6]. Several methods have been proposed to alleviate these problems. Renormalization group transformations, for instance, are routinely used to "soften" interactions [6–8], and many insights have been gained through these transformations [9]. However, such transformations of the Hamiltonian and observables [10, 11] add one layer of complexity to computations of nuclei.

One can contrast the effort of computations in the oscillator basis to, for instance, computations in nuclear lattice EFT [12]. Here, the effective interaction is tailored to the lattice spacing and, thus, to the ultraviolet (UV) cutoff, and well-known extrapolation formulas [13] can be used to estimate corrections due to finite lattice sizes. The lattice spacing is fixed once, reducing the computational expenses. This motivates us to seek a similarly efficient approach for the oscillator basis, i.e., to formulate an EFT for nuclear interactions directly in the oscillator basis.

In recent years, realistic *ab initio* nuclear computations pushed the frontier from light p-shell nuclei [14, 15] to the medium-mass regime [16–23]. At present, the precision of computational methods considerably exceeds the accuracy of available interactions [24], and this is the main limitation in pushing the frontier of *ab initio* computations to heavy nuclei. To address this situation, several efforts, ranging from new optimization protocols for chiral interactions [25–27] to the inclusion of higher orders [28, 29] to the development of interactions with novel regulators [30] are under way. To facilitate the computation of heavy nuclei we propose to tailor interactions from chiral EFT to the oscillator basis.

There exist several proposals to formulate EFTs in the oscillator basis. Haxton and coworkers proposed the oscillator based effective theory (HOBET) [31–34]. They focused on decoupling low- and high-energy modes in the oscillator basis via the Bloch-Horowitz formalism, and on the resummation of the kinetic energy to improve the asymptotics of bound-state wave functions in configuration space. The HOBET interaction is based on a contact-gradient expansion, and the matrix elements are computed in the oscillator basis. The resulting interaction exhibits a weak energy dependence. The Arizona group [35–37] posed and studied questions related to the UV and infrared (IR) cutoffs imposed by the oscillator basis, and developed a pion-less EFT in the oscillator basis. This EFT was also applied to harmonically trapped atoms [38]. In this approach, the interaction matrix elements are also based on a contact-gradient expansion and computed in the oscillator basis. Running coupling constants depend on the UV cutoff of the employed oscillator basis. In a sequence of other papers, Tölle *et al.* studied harmonically trapped few-boson systems in an effective field theory based on contact interactions with running coupling constants [39, 40].

Our oscillator EFT differs from these approaches. For the interaction we choose an oscillator space with a fixed oscillator frequency ω and a fixed maximum energy $(N_{\max} + 3/2)\,\hbar\omega$. The matrix elements of the interaction are taken from an EFT formulated in momentum space and evaluated at the discrete momentum eigenvalues of the kinetic energy in this fixed oscillator space. This reformulation, or projection, of a momentum-space EFT

onto a finite oscillator model space requires us to re-fit the low-energy coefficients (LECs) of interactions at a given order of the EFT. We determine these by an optimization to scattering phase shifts (computed in the finite oscillator basis via the J-matrix approach [41, 42]) and from deuteron properties. The power counting of the oscillator EFT is based on that of the underlying momentum-space EFT. The finite oscillator space introduces IR and UV cutoffs [35, 43–49], and these are thus fixed for the interaction.

In practical many-body calculations we will keep the oscillator frequency and the interaction fixed at $\hbar\omega$ and $N_{\max}$, but employ the kinetic energy in larger model spaces. This increase of the model space increases (decreases) its UV (IR) cutoff but does not change any interaction matrix elements and thus leaves the IR and UV cutoff of the interaction unchanged. As UV convergence of the many-body calculations depends on the matrix elements of an interaction [47], oscillator EFT guarantees this UV convergence by construction because no new potential matrix elements enter beyond $N_{\max}$. We stress that our notion of UV convergence relates to the convergence of the many-body calculations and should not be confused with the expectation that observables are independent of the regulator or cutoff. Infrared convergence builds up the exponential tail of bound-state wave functions in position space, as the effective IR cutoff of a finite nucleus is set by its radius. Thus, the increase of the model space for the kinetic energy achieves IR convergence. Regarding IR convergence, oscillator EFT is similar to the HOBET of Ref. [33]. In practice, IR-converged values for bound-state energies and radii can be obtained applying "Lüscher-like" formulas for the oscillator basis [44].

We view oscillator EFT similar to lattice EFT [12]. The latter constructs an interaction on a lattice in position space while the former builds an interaction on a discrete (but non-equidistant) mesh in momentum space. In both EFTs the UV cutoff of the interaction is fixed once and for all, and LECs are adjusted to scattering data and bound states. The increase in lattice sites achieves IR convergence in lattice EFT, while the increase of the number of oscillator shells achieves IR convergence in oscillator EFT.

As we will see, the resulting EFT interaction in the oscillator basis exhibits a fast convergence, similar to the phenomenological JISP interaction [50]. From a practical point of view, our approach to oscillator EFT allows us to employ all of the existing infrastructure developed for nuclear calculations.

The discrete basis employed in this paper is actually the basis set of a discrete variable representation (DVR) [51–57] in momentum space. While coordinate-space DVRs are particularly useful and popular in combination with local potentials, the results of this paper suggest that DVRs are also useful in momentum-space-based EFTs, because they facilitate the evaluation of matrix elements.

This paper is organized as follows. In Section II we analyze the momentum-space structure of a finite oscillator basis. In Section III we validate our approach by reproducing an interaction from chiral EFT at next-to-leading order (NLO). In Section IV we construct a NLO interaction from realistic phase shifts and employ this interaction in many-body calculations, demonstrating that converged binding energies and radii can be obtained for nuclei in the mass-100 region in model spaces with $N_{\max} = 10$ to 14 without any further renormalization. We finally present our summary in Section V.

II. THEORETICAL CONSIDERATIONS

In this Section we present the theoretical foundation of an EFT in the oscillator basis. We derive analytical expressions for the momentum eigenstates and eigenvalues in finite oscillator spaces and present useful formulas for interaction matrix elements.

A. Momentum states in finite oscillator spaces

The radial wave functions $\langle r,l|n,l\rangle = \psi_{nl}(r)$ of oscillator basis states $|n,l\rangle$ can be represented in terms of generalized Laguerre polynomials $L_n^{l+1/2}$ as

$$\psi_{n,l}(r) = (-1)^n \sqrt{\frac{2n!}{\Gamma(n+l+3/2)b^3}} \left(\frac{r}{b}\right)^l e^{-\frac{1}{2}\left(\frac{r}{b}\right)^2} L_n^{l+1/2}\left(\frac{r^2}{b^2}\right). \quad (1)$$

Here, $b \equiv \sqrt{\hbar/(m\omega)}$ is the oscillator length expressed in terms of the nucleon mass m and oscillator frequency ω. In what follows, we use units in which $\hbar = 1$.

In free space, the spherical eigenstates of the momentum operator $\hat{p}$ are denoted as $|k,l\rangle$ with k being continuous. The corresponding wave functions

$$\langle r,l|k,l\rangle = \sqrt{\frac{2}{\pi}} j_l(kr) \quad (2)$$

are spherical Bessel functions j_l up to a normalization factor. These continuum states are normalized as

$$\langle k',l|k,l\rangle = \int_0^\infty \mathrm{d}r r^2 \langle k',l|r,l\rangle\langle r,l|k,l\rangle = \frac{\delta(k-k')}{kk'}. \quad (3)$$

Introducing the momentum-space representation of the radial oscillator wave functions via the Fourier-Bessel transform

$$\tilde{\psi}_{n,l}(k) \equiv \int_0^\infty \mathrm{d}r r^2 \langle k,l|r,l\rangle \psi_{n,l}(r) \quad (4)$$
$$= \sqrt{\frac{2n!b^3}{\Gamma(n+l+3/2)}} (kb)^l e^{-\frac{1}{2}k^2b^2} L_n^{l+1/2}\left(k^2b^2\right),$$

enables us to expand the continuous momentum states (2) in terms of the oscillator wave functions

$$\langle r,l|k,l\rangle = \sum_{n=0}^{\infty} \tilde{\psi}_{n,l}(k)\psi_{n,l}(r). \tag{5}$$

As we want to develop an EFT, it is most important to understand the squared momentum operator $\hat{p}^2$. An immediate consequence of Eq. (2) is of course that the spherical Bessel functions are also eigenfunctions of $\hat{p}^2$ with corresponding eigenvalues k^2, i.e., $\hat{p}^2 j_l(kr) = k^2 j_l(kr)$. In the oscillator basis, the matrix representation of $\hat{p}^2$ is tri-diagonal, with elements

$$\begin{aligned}\langle n',l|\hat{p}^2|n,l\rangle = b^{-2}\Big[&(2n+l+3/2)\delta_n^{n'} \\ &-\sqrt{n(n+l+1/2)}\delta_n^{n'+1} \\ &-\sqrt{(n+1)(n+l+3/2)}\delta_n^{n'-1}\Big].\end{aligned} \tag{6}$$

We want to solve the eigenvalue problem of the operator $\hat{p}^2$ in a finite oscillator basis truncated at an energy $(N_{\max}+3/2)\,\hbar\omega$. For partial waves with angular momentum l the basis consists of wave functions (1) with $n = 0,\dots N$, i.e., the sum in Eq. (5) is truncated at

$$N \equiv \left[\frac{N_{\max}-l}{2}\right]. \tag{7}$$

Here $[x]$ denotes the integer part of x. While N clearly depends on l and $N_{\max}$, we will suppress this dependence in what follows. Motivated by Eq. (5) we act with the matrix of $\hat{p}^2$ on the component vector $(\tilde{\psi}_{0,l}(k),\dots,\tilde{\psi}_{N,l}(k))^T$. The well-known three-term recurrence relation for Laguerre polynomials (see, e.g., Eq. 8.971(4) of Ref. [58]) implies

$$\begin{aligned}0 = &(2n+l+3/2-b^2k^2)\,\tilde{\psi}_{n,l}(k) \\ &-\sqrt{n(n+l+1/2)}\,\tilde{\psi}_{n-1,l}(k) \\ &-\sqrt{(n+1)(n+l+3/2)}\,\tilde{\psi}_{n+1,l}(k),\end{aligned} \tag{8}$$

and for our eigenvalue problem we arrive at

$$\hat{p}^2\begin{pmatrix}\tilde{\psi}_{0,l}(k)\\ \vdots \\ \tilde{\psi}_{N-1,l}(k)\\ \tilde{\psi}_{N,l}(k)\end{pmatrix} = k^2\begin{pmatrix}\tilde{\psi}_{0,l}(k)\\ \vdots \\ \tilde{\psi}_{N-1,l}(k)\\ \tilde{\psi}_{N,l}(k)\end{pmatrix} + \begin{pmatrix}0\\ \vdots \\ 0\\ b^{-2}\sqrt{(N+1)(N+l+3/2)}\,\tilde{\psi}_{N+1,l}(k)\end{pmatrix}. \tag{9}$$

For $k = k_{\mu,l}$ such that $\tilde{\psi}_{N+1,l}(k) = 0$, the second term on the right-hand side of Eq. (9) vanishes, and we obtain an eigenstate of the momentum operator (6) in the finite oscillator space.

Thus, momenta $k_{\mu,l}$ (with $\mu = 0,\dots,N$) such that $k_{\mu,l}^2 b^2$ is a root of the the Laguerre polynomial $L_{N+1}^{l+1/2}$ solve the eigenvalue problem of the $\hat{p}^2$ operator in the finite oscillator space. We recall that $L_{N+1}^{l+1/2}$ has $N+1$ roots. Thus, in a finite model space consisting of oscillator functions with $n = 0,\dots,N$ the eigenvalues of the squared momentum operator are the $N+1$ roots $k_{\mu,l}^2$ of the Laguerre polynomial $L_{N+1}^{l+1/2}$. We note that $k_{\mu,l}$ depends on the angular momentum l as well as N. To avoid a proliferation of indices, we suppress the latter dependence in what follows. By construction, the basis built on discrete momentum eigenstates is a DVR [54–56].

Previous studies showed that the finite oscillator basis is equivalent to a spherical cavity at low energies [44], and the radius of this cavity is related to the wavelength of the discrete momentum eigenstate with lowest momentum. References [45, 46] give analytical results for the lowest momentum eigenvalue in the limit of $N \gg 1$. The exact determination of the eigenvalues of the momentum operator in the present work allows us to give exact values for the radius of the cavity corresponding to the finite oscillator basis. This radius is relevant because it enters IR extrapolations [43, 45, 46]. Let $k_{0,l}^2 b^2$ be the smallest root of the Laguerre polynomial $L_{N+1}^{l+1/2}$, and let $z_{0,l}$ denote the smallest root of the spherical Bessel function j_l. Then

$$\frac{z_{0,l}}{L(N,l)} = k_{0,l} \tag{10}$$

defines the effective radius L we seek.

The radial momentum eigenfunction corresponding to the eigenvalue $k_{\mu,l}$ in the partial wave with angular momentum l has an expansion of the form

$$\phi_{\mu,l}(r) \equiv c_{\mu,l}\sum_{n=0}^{N}\tilde{\psi}_{n,l}(k_{\mu,l})\psi_{n,l}(r). \tag{11}$$

This wave function is the projection of the spherical Bessel function (5) onto the finite oscillator space. It is also an eigenfunction of the momentum operator projected onto the finite oscillator space because the specific values of $k_{\mu,l}$ decouple this wave function from the excluded space. In Eq. (11) $c_{\mu,l}$ is a normalization constant that we need to determine. In order to do so we consider

the overlap

$$\langle\phi_{\mu,l}|\phi_{\nu,l}\rangle = \int_0^\infty \mathrm{d}r r^2 \phi_{\mu,l}(r)\phi_{\nu,l}(r) \tag{12}$$
$$= c_{\mu,l}c_{\nu,l}\sum_{n=0}^{N}\tilde{\psi}_{n,l}(k_{\mu,l})\tilde{\psi}_{n,l}(k_{\nu,l})$$
$$= c_{\mu,l}c_{\nu,l}\sqrt{(N+1)(N+l+3/2)}$$
$$\times\frac{\tilde{\psi}_{N,l}(k_{\mu,l})\tilde{\psi}_{N+1,l}(k_{\nu,l}) - \tilde{\psi}_{N+1,l}(k_{\mu,l})\tilde{\psi}_{N,l}(k_{\nu,l})}{(k_{\mu,l}^2 - k_{\nu,l}^2)b^2}.$$

Here, we used the Christoffel-Darboux formula for orthogonal polynomials, see, e.g., Eq. 8.974(1) of Ref. [58]. As $k_{\mu,l}$ and $k_{\nu,l}$ are roots of $\tilde{\psi}_{N+1,l}$, we confirm orthogonality. For $k_{\mu,l} = k_{\nu,l}$ we use the rule by l'Hospital and find (with help of Eq. 8.974(2) of Ref. [58])

$$c_{\mu,l}^{-1} = \frac{\sqrt{(N+1)(N+l+3/2)}}{k_{\mu,l}b}\tilde{\psi}_{N,l}(k_{\mu,l}). \tag{13}$$

It is also useful to compute the overlap

$$\langle k_{\mu,l}, l|\phi_{\nu,l}\rangle = \sqrt{\frac{\pi}{2}}\int_0^\infty \mathrm{d}r r^2 j_l(k_{\mu,l}r)\phi_{\nu,l}(r)$$
$$= \delta_\mu^\nu c_{\mu,l}^{-1}. \tag{14}$$

This overlap vanishes for $k_{\mu,l} \neq k_{\nu,l}$, thus, the eigenstates of the $\hat{p}^2$ operator in finite oscillator spaces are orthogonal to the continuous momentum eigenstates when the latter are evaluated at the discrete momenta. This exact result is very useful for the computation of matrix elements of a potential operator $\hat{V}$.

For arbitrary continuous momenta k we obtain from Eq. (12)

$$\tilde{\phi}_{\nu,l}(k) \equiv \langle k, l|\phi_{\nu,l}\rangle = \frac{k_{\nu,l}/b}{k_{\nu,l}^2 - k^2}\tilde{\psi}_{N+1,l}(k). \tag{15}$$

The wave function (15) is the Fourier-Bessel transform of the discrete radial momentum wave function $\phi_{\nu,l}(r)$. We note that Eq. (11) relates the discrete momentum eigenfunctions to the oscillator eigenstates via an orthogonal transformation, implying

$$\sum_{\mu=0}^{N} c_{\mu,l}^2 \tilde{\psi}_{n,l}(k_{\mu,l})\tilde{\psi}_{n',l}(k_{\mu,l}) = \delta_{n'}^n, \tag{16}$$

and

$$\sum_{n=0}^{N} \tilde{\psi}_{n,l}(k_{\mu,l})\tilde{\psi}_{n,l}(k_{\nu,l}) = \delta_\mu^\nu c_{\mu,l}^{-2}. \tag{17}$$

We remind the reader that the discrete set of momenta $k_{\mu,l}$ is fixed once a particular N is chosen. Equation (16) can be used to relate oscillator basis functions to the discrete momentum eigenfunctions (11). Thus,

$$\psi_{n,l}(r) = \sum_{\mu=0}^{N} c_{\mu,l}\tilde{\psi}_{n,l}(k_{\mu,l})\phi_{\mu,l}(r). \tag{18}$$

B. Matrix elements of interactions from EFT

Nucleon-nucleon (NN) interactions from EFT are typically available for continuous momenta in a partial-wave basis in form of the matrix elements $\langle k', l'|\hat{V}|k, l\rangle$. Numerical integration techniques are used to transform these matrix elements into the oscillator basis. However, there is a very simple approximative relationship between the matrix elements with continuous momenta and the matrix elements $\langle\phi_{\nu,l'}|\hat{V}|\phi_{\mu,l}\rangle$ in the discrete momentum basis. This relationship is motivated by EFT arguments and we use it in our applications of oscillator EFT. We consider the matrix element

$$\langle k', l'|\hat{V}|\phi_{\mu,l}\rangle = \int_0^\infty \mathrm{d}k k^2 \langle k', l'|\hat{V}|k, l\rangle\langle k, l|\phi_{\mu,l}\rangle$$
$$= \frac{1}{2b^3}\int_0^\infty dx x^{l+1/2}e^{-x}$$
$$\times\left(\langle k', l'|\hat{V}\frac{|x^{1/2}b^{-1}, l\rangle\langle x^{1/2}b^{-1}, l|}{x^l e^{-x}}|\phi_{\mu,l}\rangle\right). \tag{19}$$

Here, we introduced the dimensionless integration variable $x \equiv b^2k^2$ and factored out a weight function $x^{l+1/2}e^{-x}$ from the integrand (given in brackets) in preparation for the next step. We evaluate the integral using $(N+1)$-point generalized Gauss-Laguerre quadrature based on the selected weight function. Thus, the matrix element (19) becomes

$$\langle k', l'|\hat{V}|\phi_{\mu,l}\rangle =$$
$$\frac{1}{2b^3}\sum_{\nu=0}^{N} w_{\nu,l}\langle k', l'|\hat{V}|x_{\nu,l}^{1/2}b^{-1}, l\rangle\frac{\langle x_{\nu,l}^{1/2}b^{-1}, l|\phi_{\mu,l}\rangle}{x_{\nu,l}^l e^{-x_{\nu,l}}} \tag{20}$$
$$+\Delta_{N+1}.$$

Here, $x_{\nu,l}$ are the roots of the Laguerre polynomial $L_{N+1}^{l+1/2}$, the weights are

$$w_{\nu,l} \equiv \frac{\Gamma(N+l+5/2)x_{\nu,l}}{(N+1)!\left[(N+2)L_{N+2}^{l+1/2}(x_{\nu,l})\right]^2}$$
$$= \frac{\Gamma(N+l+3/2)x_{\nu,l}}{(N+1)!(N+l+3/2)\left[L_N^{l+1/2}(x_{\nu,l})\right]^2}, \tag{21}$$

and the error term is

$$\Delta_{N+1} \equiv \frac{(N+1)!\Gamma(N+l+5/2)}{(2N+1)!}f^{(2N+2)}(\xi), \tag{22}$$

see, e.g., Ref. [59]. For the weights, we also used Eq. 8.971(6) of Ref. [58]. In the error term, $f^{(2N+2)}(\xi)$ denotes the $(2N+2)$-th derivative of the integrand (given in round brackets) of Eq. (19), evaluated at ξ which is somewhere in the integration domain.

We want to estimate the order of the error term Δ_{N+1} when using EFT interactions. For this purpose, we write

the potential as a sum of separable potentials

$$V(k',k) = \sum_a v_a g_a(k') g_a(k), \tag{23}$$

and write

$$g_a(k) = (k/\Lambda)^l e^{-\frac{1}{2}k^2 b^2} \tilde{g}_a(k/\Lambda). \tag{24}$$

Here, Λ is a high-momentum cutoff. The function $\tilde{g}_a(k/\Lambda)$ is an even function of its arguments (see, e.g., Ref. [2]), and can be expanded in a Taylor series

$$\tilde{g}_a(k) = \sum_{n=0}^{\infty} \frac{\tilde{g}_a^{(n)}(0)}{n!} \left(\frac{x}{\Lambda^2 b^2}\right)^n. \tag{25}$$

Here, we again used $x \equiv b^2 k^2$. With this expansion in mind, and noting that the wave function $\tilde{\phi}_{\nu,l}$ can be expanded in terms of oscillator wave functions, the integrand f (given in round brackets) of Eq. (19) is a product of $\tilde{g}_a$ and a sum of Laguerre polynomials (from the wave function $\tilde{\phi}_{\nu,l}$). The $(N+1)$-point Gauss-Laguerre integration is exact for monomials up to x^{2N+1}. As the wave function $\tilde{\phi}_{\nu,l}$ contains monomials up to x^N, the Gauss-Laguerre integration becomes inexact for terms starting at $n = N+2$ in the Taylor series (25). Thus, $f^{(2N+2)}$ in the error term (22) scales as $1/(\Lambda b)^{2N+l+4}$. In the oscillator EFT, typical momenta k scale as $1/b$, and the error term scales as

$$\Delta_{N+1} = \mathcal{O}\left((k/\Lambda)^{2N+l+4}\right). \tag{26}$$

Therefore,

$$\langle k',l'|\hat{V}|\phi_{\mu,l}\rangle = \langle k',l'|\hat{V}|k_{\mu,l},l\rangle c_{\mu,l} + \mathcal{O}\left((k/\Lambda)^{2N+l+4}\right). \tag{27}$$

Repeating the calculation for the bra side yields the final result

$$\langle \phi_{\nu,l'}|\hat{V}|\phi_{\mu,l}\rangle = c_{\nu,l'} c_{\mu,l} \langle k_{\nu,l'},l'|\hat{V}|k_{\mu,l},l\rangle + \mathcal{O}\left((k/\Lambda)^{2N+l+4}\right). \tag{28}$$

In oscillator EFT, we will omit the correction term and set

$$\langle \phi_{\nu,l'}|\hat{V}|\phi_{\mu,l}\rangle = c_{\nu,l'} c_{\mu,l} \langle k_{\nu,l'},l'|\hat{V}|k_{\mu,l},l\rangle. \tag{29}$$

We note that this assignment seems to be very natural for an EFT built on a finite number of discrete momentum states. For sufficiently large N, the difference to the matrix element obtained from an exact integration can be view as a correction that is beyond the order of the power counting of the EFT we build upon. In Eq. (29) the matrix elements between the discrete and continuous momentum states simply differ by normalization factors because of the different normalization (14) of discrete and continuous momentum eigenstates. Thus, partial-wave decomposed matrix elements of any momentum-space operator can readily be used to compute the corresponding oscillator matrix elements. In the Appendix we present an alternative motivation for the usage of Eq. (29).

In the remainder of this Subsection, we give useful formulas that relate the matrix elements and wave functions of the discrete momentum basis and the oscillator basis. We note that the oscillator basis states $|\psi_{n,l}\rangle$ are related to the discrete momentum states $|\phi_{n,l}\rangle$ via Eq. (18). Thus, we can also give an useful formula that transforms momentum-space matrix elements to the oscillator basis according to

$$\langle \psi_{n',l'}|\hat{V}|\psi_{n,l}\rangle = \tag{30}$$
$$\sum_{\nu,\mu=0}^{N} c^2_{\nu,l'} \tilde{\psi}_{n',l'}(k_{\nu,l'}) \langle k_{\nu,l'},l'|\hat{V}|k_{\mu,l},l\rangle c^2_{\mu,l} \tilde{\psi}_{n,l}(k_{\mu,l}) + \mathcal{O}\left(k^{2N+2}\right). \tag{31}$$

This formula also reflects the well known fact that the oscillator basis mixes low- and high-momentum physics.

The relation between matrix elements in the oscillator basis and the discrete momentum basis is given by

$$\langle \phi_{\nu,l'}|\hat{V}|\phi_{\mu,l}\rangle = c_{\nu,l'} c_{\mu,l} \sum_{n,n'=0}^{N} \tilde{\psi}_{n',l'}(k_{\nu,l'}) \langle \psi_{n',l'}|\hat{V}|\psi_{n,l}\rangle \tilde{\psi}_{n,l}(k_{\mu,l}). \tag{32}$$

Finally, we discuss the inversion of Eq. (30), e.g., for situations where scattering processes in the continuum have to be considered for interactions based on oscillator spaces. We obtain

$$\langle k_{\nu,l'},l'|\hat{V}|k_{\mu,l},l\rangle = \sum_{n,n'=0}^{N} \tilde{\psi}_{n',l'}(k_{\nu,l'}) \langle \psi_{n',l'}|\hat{V}|\psi_{n,l}\rangle \tilde{\psi}_{n,l}(k_{\mu,l}) + \mathcal{O}\left(k^{2N+l+4}\right), \tag{33}$$

because of Eq. (17).

For arbitrary momenta, one needs to use the overlaps (15) in the evaluation of the matrix elements, and finds the generalization of Eq. (33) as

$$\langle k',l'|\hat{\Pi}\hat{V}\hat{\Pi}|k,l\rangle = \tilde{\psi}_{N+1,l'}(k') \tilde{\psi}_{N+1,l}(k) \times \sum_{\nu,\mu=0}^{N} \frac{k_{\nu,l'}/b}{(k')^2 - k^2_{\nu,l'}} \langle \phi_{\nu,l'}|\hat{V}|\phi_{\mu,l}\rangle \frac{k_{\mu,l}/b}{k^2 - k^2_{\mu,l}}. \tag{34}$$

Here, we introduced the projection operator onto the finite oscillator space

$$\hat{\Pi} \equiv \sum_{\nu=0}^{N} \sum_{l=0}^{N_{\max}-2\nu} |\phi_{\nu,l}\rangle\langle\phi_{\nu,l}|. \tag{35}$$

We note that the projection operator acts as a UV (and IR) regulator. It is nonlocal, and can be written in many

ways. Examples are

$$\langle k',l|\hat{\Pi}|k,l\rangle = \sum_{n=0}^{N} \tilde{\psi}_{n,l}(k')\tilde{\psi}_{n,l}(k) \tag{36}$$

$$= \frac{\sqrt{(N+1)(N+l+3/2)}}{b^2} \times \frac{\tilde{\psi}_{N,l}(k)\tilde{\psi}_{N+1,l}(k') - \tilde{\psi}_{N+1,l}(k)\tilde{\psi}_{N,l}(k')}{k^2-(k')^2} \tag{37}$$

$$= \frac{\tilde{\psi}_{N+1,l}(k')\tilde{\psi}_{N+1,l}(k)}{b^2} \times \sum_{\nu=0}^{N} \frac{k_{\nu,l}^2}{[(k')^2-k_{\nu,l}^2][k^2-k_{\nu,l}^2]}. \tag{38}$$

Here, the first identity comes directly from the definition of the projector in terms of the oscillator eigenfunctions. The second identity follows from the calculation displayed in Eq. (12), while the third identity follows from Eq. (15).

This presents us with an alternative motivation (but not derivation) of Eq. (29). We evaluate the projected matrix elements (34) at discrete momenta and find with Eq. (15) that

$$\langle k_{\nu,l'},l'|\hat{\Pi}\hat{V}\hat{\Pi}|k_{\mu,l},l\rangle = c_{\nu,l'}^{-1}c_{\mu,l}^{-1}\langle\phi_{\nu,l'}|\hat{V}|\phi_{\mu,l}\rangle. \tag{39}$$

We note that

$$\langle k_{\nu,l'},l'|\hat{\Pi}\hat{V}\hat{\Pi}|k_{\mu,l},l\rangle = \langle k_{\nu,l'},l'|\hat{V}|k_{\mu,l},l\rangle \tag{40}$$

approximately holds for the discrete momenta in the finite oscillator space (cf. Eq. (28)).

III. CHIRAL INTERACTIONS IN FINITE OSCILLATOR BASES

In this Section we present a proof-of-principle construction of a chiral NN interaction in the framework of the oscillator EFT. First, we study the effects that the truncation to a finite oscillator basis has on phase shifts of existing NN interactions. Second, we demonstrate that a momentum-space chiral interaction at NLO can be equivalently constructed in oscillator EFT.

We consider the chiral interactions $\mathrm{N^3LO_{EM}}$ [60] and $\mathrm{NLO_{sim}}$ [27]. Both interactions employ regulators of the form

$$f(q) = \exp\left[-\left(\frac{q}{\Lambda_\chi}\right)^{2n}\right]. \tag{41}$$

Here, q is a relative momentum, n is an integer, and Λ_χ is the high-momentum cutoff, specifically $\Lambda_\chi = 500$ MeV. We use $n = 3$ in what follows. This cutoff needs to be distinguished from the (hard) UV cutoff [47]

$$\Lambda_{\mathrm{UV}} \approx \sqrt{2\,(N_{\max}+7/2)}/b \tag{42}$$

of the oscillator-EFT interaction.

Let us comment on using the projector (35) in combination with the regulator (41). In momentum space, the projector (35) is approximately the identity operator for momenta k, k' between the IR and UV cutoffs Λ_{IR} and Λ_{UV} of the oscillator basis. For momenta $k, k' > \Lambda_{\mathrm{UV}}$ the projector (35) falls off as a Gaussian. For the regulator (41) we choose $\Lambda_\chi < \Lambda_{\mathrm{UV}}$, which introduces a super-Gaussian falloff for momenta $\Lambda_\chi \lesssim q \lesssim \Lambda_{\mathrm{UV}}$. As an example, let us consider $\Lambda_\chi = 500$ MeV and $\Lambda_{\mathrm{UV}} = 700$ MeV. Then, $f(\Lambda_{\mathrm{UV}}) \approx 5\times10^{-4}$ at the point where the super-Gaussian falloff goes over into a Gaussian falloff. Assuming a ratio $q/\Lambda_\chi = 1/3$ that is typical for the power counting in chiral EFT, $f(\Lambda_{\mathrm{UV}}) \approx (1/3)^7$, and the asymptotic Gaussian falloff is not expected to introduce significant contributions to contact interactions at NLO. Eventually, one might want to consider removing the regulator from an oscillator-based EFT. At this moment however, it is also useful in taming the oscillations discussed below and shown in Fig. 1.

A. Effects of finite oscillator spaces on phase shifts

It is instructive to study the effects that a projection onto a finite oscillator basis has on phase shifts. For this purpose, we employ the well known NN interaction $\mathrm{N^3LO_{EM}}$ [60]. First, we transform its matrix elements to a finite oscillator space using numerically exact quadrature, and subsequently compute the phase shifts using the J-matrix approach of Ref. [42]. The two parameter combinations $N_{\max} = 10$, $\hbar\omega = 40$ MeV, and $N_{\max} = 20$, $\hbar\omega = 23$ MeV respectively yield a UV cutoff $\Lambda_{\mathrm{UV}} \approx 700$ MeV, see Eq. (42). This considerably exceeds the high-momentum cutoff Λ_χ of the interaction. Figure 1 shows the resulting phase shifts in selected partial waves. The projection onto finite oscillator bases introduces oscillations in the phase shifts. On the one hand, many *ab initio* calculations of atomic nuclei yield practically converged results for bound-state observables in model spaces with $N_{\max} \lesssim 14$ and oscillator frequencies around 24 MeV. On the other hand, oscillator spaces consisting of only 10 to 20 shells are clearly too small to capture all the information contained in the original interaction. We note (i) that the $\mathrm{N^3LO_{EM}}$ interaction is formulated for arbitrary continuous momenta whereas oscillator EFT limits the evaluation to a few discrete momenta, and (ii) that the present Λ_{UV} cuts off the high-momentum tails of the $\mathrm{N^3LO_{EM}}$ interaction.

For $N_{\max} \to \infty$ we expect to arrive at the original phase shifts, and this is supported in Fig. 1 by the reduced oscillations in the $N_{\max} = 20$ phase shifts compared to their $N_{\max} = 10$ counterparts. The period of oscillations is approximately given by the IR cutoff. In the bottom panel of Fig. 1, the oscillator spacing $\hbar\omega$ is increased to 80 MeV (for $N_{\max} = 10$) and 46 MeV (for $N_{\max} = 20$), respectively, yielding a UV cutoff $\Lambda_{\mathrm{UV}} \approx 1000$ MeV in the oscillator basis. The phase shift oscillations are significantly reduced for such large

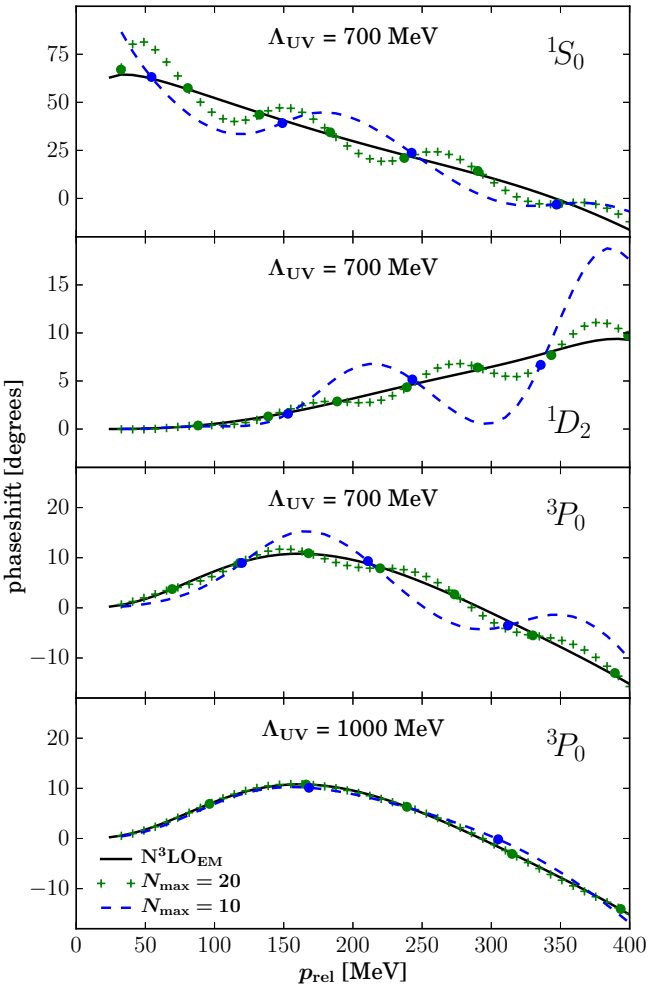

FIG. 1. (Color online) Computed np phase shifts of the NN potential N^{3}LO$_{\rm EM}$ [60] projected onto finite oscillator spaces with $N_{\rm max} = 10$ and $N_{\rm max} = 20$ compared to the phase shifts from the full (i.e., not projected) interaction in selected partial waves as a function of the relative momentum. In the top three panels the oscillator frequencies were chosen as $\hbar\omega = 40$ MeV and 23 MeV, respectively, in order to obtain an oscillator cutoff $\Lambda_{\rm UV} \approx 700$ MeV that well exceeds the chiral cutoff $\Lambda_\chi = 500$ MeV. The filled circles mark the phase shifts at the momenta corresponding to the eigenenergies of the scattering channel in the truncated oscillator space. In the bottom panel $\hbar\omega$ is increased to 80 MeV (for $N_{\rm max} = 10$) and 46 MeV (for $N_{\rm max} = 20$), respectively. This yields a UV cutoff $\Lambda_{\rm UV} \approx 1000$ MeV in the oscillator basis and significantly reduces the phase shift oscillations.

values of $\Lambda_{\rm UV}$.

We note that the eigenvalues of the Hamiltonian matrix in $(N_{\rm max}+1)$ oscillator shells play a special role for the phase shifts in uncoupled partial wave channels. At these energies, the eigenfunctions are standing waves with a Dirichlet boundary condition at the (energy-dependent) radius of the spherical cavity that is equivalent to the finite oscillator basis, and one can alternatively use this information in the computation of the phase shifts [45, 61]. The filled circles in Fig. 1 indicate the values of the phase shifts at these energies, which are close to those of the original interaction.

Subsection II B discusses two ways of projecting momentum-space interactions onto a finite oscillator space. The first approach involves the determination of the matrix element (19) via an exact numerical integration over continuous momenta. The second approach, Eq. (29), uses $(N+1)$-point Gauss-Laguerre quadrature to compute the integral in Eq. (19). This only requires us to evaluate the interaction at those momenta that are physically realized in the finite oscillator basis, which is more in the spirit of an EFT. Because we want to follow the oscillator EFT approach in later sections, we study the effect that the error term (22) associated with the $(N+1)$-point Gauss-Laguerre quadrature has on the projected phase shifts. Figure 2 shows a comparison of projected N^{3}LO$_{\rm EM}$ phase shifts obtained from the two projection approaches to the original N^{3}LO$_{\rm EM}$ phase shifts. Overall, both versions yield very similar phase shifts. For the phase shifts associated with the $(N+1)$-point Gauss-Laguerre quadrature, the oscillations seem to be somewhat reduced for small energies. Also, we find a notably improved agreement between the $(N+1)$-point Gauss-Laguerre phase shifts and the original ones at the discrete eigenenergies of the scattering channel Hamiltonians, as indicated by the full circles. From now on we exclusively use the $(N+1)$-point Gauss-Laguerre integration to compute matrix elements in oscillator EFT.

B. Reproduction of the phase shifts of a NLO interaction

In what follows we employ the oscillator EFT at NLO. All matrix elements in oscillator EFT are based on Eq. (29), i.e., the matrix elements from continuum momentum space are evaluated at the discrete momenta of the finite oscillator basis. At this order the chiral interactions depend on 11 LECs and exhibit sufficient complexity to qualitatively describe nuclear properties. Specifically, in this Section we aim at reproducing the phase shifts and selected deuteron properties of the chiral interaction NLO$_{\rm sim}$ [27] by optimizing these 11 LECs. Throughout this work, the χ^2 fits evaluate the phase shifts at 20 equidistant energies in the laboratory energy range up to 350 MeV, with weights $\sigma^2 \propto (q/\Lambda_\chi)^3$. We note that more sophisticated weights (including also the pion mass or the oscillatory patterns) would be needed for a quantification of uncertainties, see, e.g. Refs. [27, 62, 63]. In this work we only investigate the feasibility of an oscillator EFT with regard to the computation of heavy nuclei.

The main goal of oscillator EFT is to enable the computation of heavy nuclei. Therefore, we set $N_{\rm max} = 10$ for the interaction. This allows us to perform IR extrapolations based on calculations in spaces with $N_{\rm max} = 10$, 12, and 14 for the kinetic energy. To determine $\hbar\omega$ we study

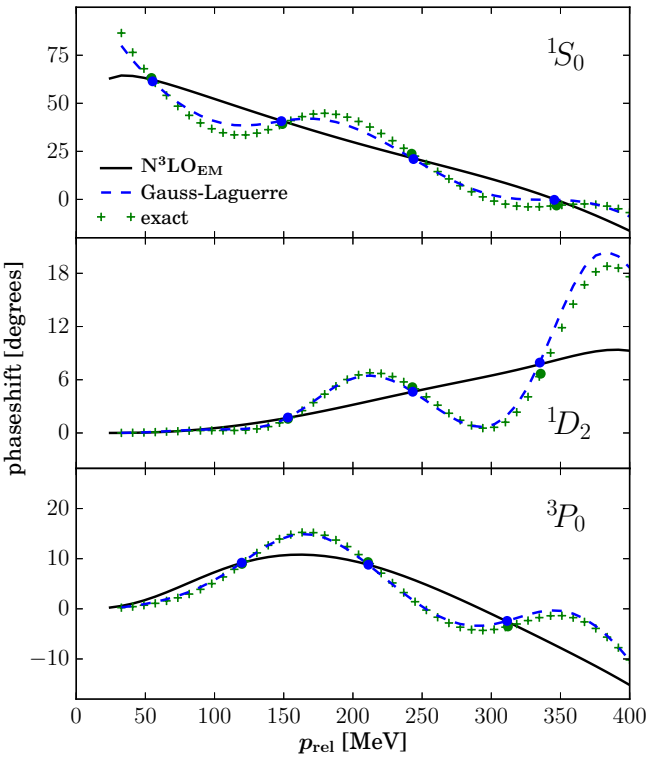

FIG. 2. (Color online) Phase shifts of N^{3}LO$_{\rm EM}$ obtained from a projection onto a $N_{\rm max} = 10$, $\hbar\omega = 40$ MeV oscillator space using (i) exact integration in Eq. (19) (blue, dashed line) and (ii) Gauss-Laguerre quadrature Eq. (29) (green crosses), compared to the unprojected N^{3}LO$_{\rm EM}$ phase shifts (black, solid line). The filled circles mark the phase shifts at the momenta corresponding to the eigenenergies of the scattering channel in the truncated oscillator space.

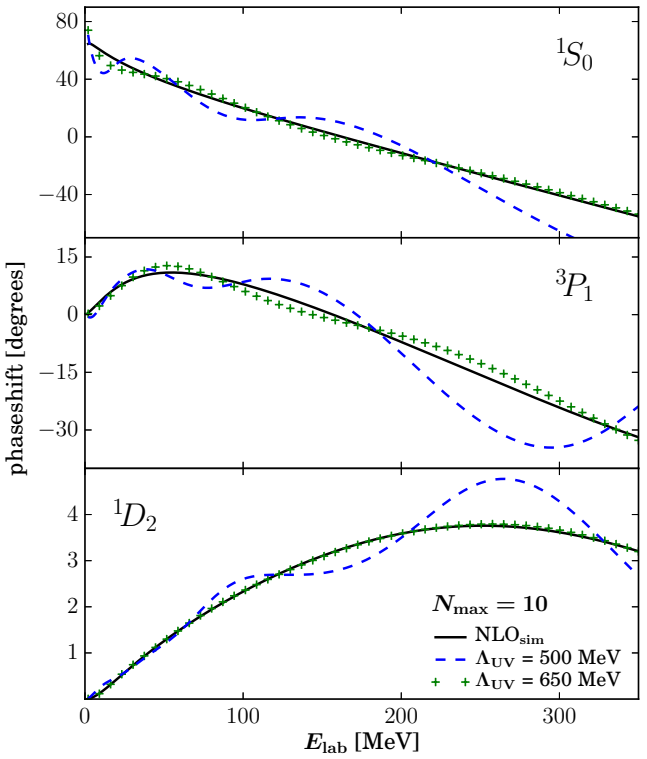

FIG. 3. (Color online) Phase shifts of NLO interactions obtained from oscillator EFT through fits to NLO$_{\rm sim}$ phase shifts compared to the NLO$_{\rm sim}$ data [27]. The momentum-space interaction matrix elements used in the construction of the oscillator EFT interactions employ a fixed chiral cutoff $\Lambda_\chi = 500$ MeV. We fix $N_{\rm max} = 10$ and consider the two oscillator frequencies $\hbar\omega = 20$ MeV and 34 MeV, yielding UV cutoffs $\Lambda_{\rm UV} = 500$ MeV and 650 MeV, respectively. For $\Lambda_{\rm UV} = 650$ MeV, the oscillations in the phase shifts are notably reduced.

phase shifts in selected partial waves in Fig. 3. The first value, $\hbar\omega = 20$ MeV, again corresponds to a UV cutoff of $\Lambda_{\rm UV} \approx 500$ MeV and yields the familiar oscillations in the phase shifts. The second value, $\hbar\omega = 34$ MeV, corresponds to a UV cutoff $\Lambda_{\rm UV} \approx 650$ MeV that significantly exceeds the chiral cutoff $\Lambda_\chi \approx 500$ MeV. In this case, the oscillations are drastically reduced. Consequently, we use $\hbar\omega = 34$ MeV in the following.

In Fig. 4 we compare further phase shifts from the oscillator EFT to the NLO$_{\rm sim}$ phase shifts. We note that the channel $^1D_2$ is a prediction because there is no corresponding LEC at this chiral order. For completeness, and to assess the large-$N_{\rm max}$ behavior, we also show the results of an optimization in oscillator EFT with $N_{\rm max} = 80$ and $\hbar\omega = 6$ MeV ($\Lambda_{\rm UV} \approx 650$ MeV) as green crosses. In general, oscillator EFT reproduces the phase shifts well over the whole energy range up to the pion-production threshold.

In the deuteron channel we fit not only to phase shifts but also to its binding energy E_d, point-proton radius r_d, and quadrupole moment Q_d. For $N_{\rm max} = 80$, we reproduce the deuteron properties well, as can be seen in Table I. For the $N_{\rm max} = 10$ effective interaction, it becomes more difficult to simultaneously reproduce all data. Therefore, we relax the requirement to reproduce the quadrupole moment in favor of the other deuteron properties and the phase shifts. We converge the deuteron calculations by employing large model spaces of 100 oscillator shells where only the kinetic energy acts beyond the $N_{\rm max}$ used to define the effective interaction.

In Table I we also compare the LECs of the effective interactions for $N_{\rm max} = 10$ and 80 to the LECs of NLO$_{\rm sim}$. For $N_{\rm max} = 80$, our approach quite accurately reproduces the NLO$_{\rm sim}$ LECs, with $C_{^3S_1}$ being the only exception. Because this LEC is associated with the deuteron channel, its value is affected by the weighting of the deuteron properties in the fit, and we expect that a better reproduction can be achieved by assigning different weights to the deuteron properties. More importantly, with the exception of $C_{^3S_1}$, the values of the LECs for the $N_{\rm max} = 10$ interaction are very similar to the LECs of the NLO$_{\rm sim}$ interaction. Also, all of the values are of natural size.

Let us also address the sensitivity of our results to the

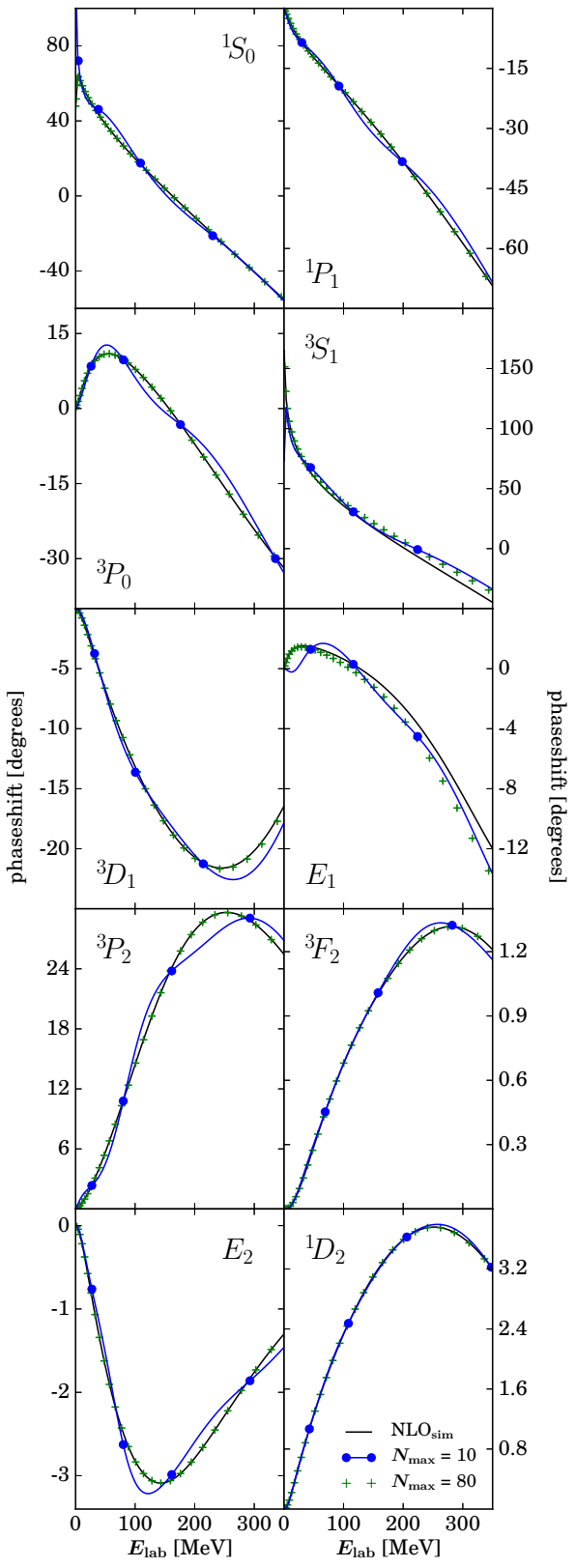

FIG. 4. (Color online) Phase shifts from oscillator EFT with $N_{\rm max} = 10$ (full blue circles and blue line) compared to NLO$_{\rm sim}$ phase shifts (black line) for partial wave channels as indicated. Also shown (green crosses) are results from oscillator EFT in a large model space with $N_{\rm max} = 80$.

	$N_{\rm max} = 10$	$N_{\rm max} = 80$	NLO$_{\rm sim}$
E_d [MeV]	−2.268	−2.212	−2.225
r_d [fm]	2.108	1.962	1.976
Q_d [fm^2]	0.195	0.259	0.259
P_d	0.028	0.029	0.029
$\tilde{C}^{(np)}_{^1S_0}$	−0.157499	−0.150552	−0.150623
$\tilde{C}^{(pp)}_{^1S_0}$	−0.15513	−0.14877	−0.14891
$\tilde{C}^{(nn)}_{^1S_0}$	−0.15645	−0.14990	−0.14991
$C_{^1S_0}$	1.7972	1.6910	1.6935
$\tilde{C}_{^3S_1}$	−0.1721	−0.1752	−0.1843
$C_{^3S_1}$	−0.406	−0.389	−0.218
C_{E_1}	0.224	0.232	0.263
$C_{^3P_0}$	1.3038	1.2995	1.2998
$C_{^1P_1}$	1.047	1.023	1.025
$C_{^3P_1}$	−0.335	−0.336	−0.336
$C_{^3P_2}$	−0.2010	−0.2028	−0.2029

TABLE I. Comparison of deuteron properties and LECs for effective interactions with $N_{\rm max} = 10$, 80 obtained from a fit to NLO$_{\rm sim}$ phase shifts and deuteron properties, compared to NLO$_{\rm sim}$ data [27]. The deuteron properties, computed in large $N_{\rm max} = 100$ model spaces, are the ground-state energy E_d, point-proton radius r_d, quadrupole moment Q_d, and D-state probability P_d. The oscillator frequencies $\hbar\omega$ are 34 MeV and 6 MeV, respectively, corresponding to a UV cutoff of $\Lambda_{\rm UV} \approx 650$ MeV.

UV cutoff of the employed oscillator space. For this purpose we keep $\hbar\omega = 34$ MeV fixed and optimize two more interactions defined in model spaces with $N_{\rm max} = 12$ and $N_{\rm max} = 14$, respectively. We recall that the UV cutoff of the model space increases with increasing $N_{\rm max}$, and that $N_{\rm max} = 10, 12, 14$ corresponds to UV cutoff $\Lambda_{\rm UV} \approx 650$, 700, 750 MeV, respectively. Resulting few-body observables from these interactions are shown in Table II, and also compared to the infinite-space interaction NLO$_{\rm sim}$. We see that results converge slowly toward those of the NLO$_{\rm sim}$ interaction as $N_{\rm max}$ is increased. We also note that the few-body observables from the different $N_{\rm max}$ interactions exhibit differences that are consistent with uncertainty expectations at NLO [27, 29, 64].

Clearly, the NLO interaction from oscillator EFT differs from NLO$_{\rm sim}$ through the complicated projection that introduces IR and UV cutoffs and is highly nonlocal, see Eq. (35). In the EFT sense the difference between these interactions should be beyond the order at which we are currently operating. While we cannot prove this equivalence, the numerical results of this Section encourage us to pursue the construction of a chiral NLO interaction within oscillator EFT by optimization to the phase shifts from a high-precision NN potential in the following Section.

	$N_{\max}=10$	$N_{\max}=12$	$N_{\max}=14$	$\mathrm{NLO_{sim}}$
E_d	-2.261	-2.227	-2.225	-2.224
r_d	2.108	1.974	1.889	1.975
Q_d	0.195	0.279	0.272	0.259
P_d	0.028	0.031	0.031	0.028
$E_{^3\mathrm{H}}$	-8.944	-8.502	-8.094	-8.270
$r_{^3\mathrm{H}}$	1.627	1.592	1.578	1.614
$E_{^3\mathrm{He}}$	-8.169	-7.735	-7.33	-7.528
$r_{^3\mathrm{He}}$	1.787	1.764	1.761	1.791
$E_{^4\mathrm{He}}$	-28.736	-27.96	-27.302	-27.44
$r_{^4\mathrm{He}}$	1.465	1.463	1.457	1.482

TABLE II. Deuteron properties as in Table I, as well as binding energies (in MeV) and radii (in fm) for ^{3}H, ^{3}He, and ^{4}He from different effective interactions, compared to $\mathrm{NLO_{sim}}$. The oscillator length $\hbar\omega$ is fixed at 34 MeV, and we consider $N_{\max}=10,\,12,\,14$, corresponding to values of the UV cutoff $\Lambda_{\mathrm{UV}}\approx 650,\,700,\,750$ MeV.

IV. NLO INTERACTIONS IN OSCILLATOR EFT AND MANY-BODY RESULTS

In what follows, we set $N_{\max}=10$ for the interaction. On the one hand, lower oscillator frequencies correspond to larger oscillator lengths and lead to a rapid IR convergence. On the other hand, lower oscillator frequencies also correspond to lower UV cutoffs. In what follows we choose $\hbar\omega=24$ MeV which results in a UV cutoff $\Lambda_{\mathrm{UV}}\approx 550$ MeV and an IR length $L\approx 9.6$ fm according to Eq. (10). Considering the tail of the regulator function (41) we set $\Lambda_\chi=450$ MeV, which ensures that Λ_{UV} significantly exceeds Λ_χ.

Practical calculations are performed in the laboratory system, and use the $N_{\max}=10$ interaction together with the intrinsic kinetic energy in oscillator spaces with $N^{\mathrm{lab}}=2n_1+l_1\geq N_{\max}$. Here n_1 and l_1 are the radial and angular momentum quantum numbers of the harmonic oscillator in the laboratory frame. Results for $N^{\mathrm{lab}}=10,12,14$ are feasible and will allow us to perform IR extrapolations for bound-state energies and radii.

In this Section, we construct a chiral interaction at NLO from realistic phase shifts, and subsequently utilize it in coupled-cluster calculations of ^{4}He, ^{16}O, ^{40}Ca, ^{90}Zr, and ^{132}Sn. Our main objectives are (i) to present a proof-of-principle optimization of a realistic interaction within the framework of the oscillator EFT, and (ii) to demonstrate that such an interaction converges fast even in heavy nuclei. We compute the matrix elements in oscillator EFT, i.e., based on Eq. (29) and omit the high-order correction terms.

In the optimization, the low-energy coefficients are obtained from a χ^2 fit to realistic scattering data (represented here by phase shifts from the CD-Bonn potential [65]) and deuteron properties. The fitting procedure is identical to the one described in Section III. Figure 5 presents the resulting phase shifts for a selection of scattering channels. We reproduce the phase shifts over a large energy range for several partial waves. The

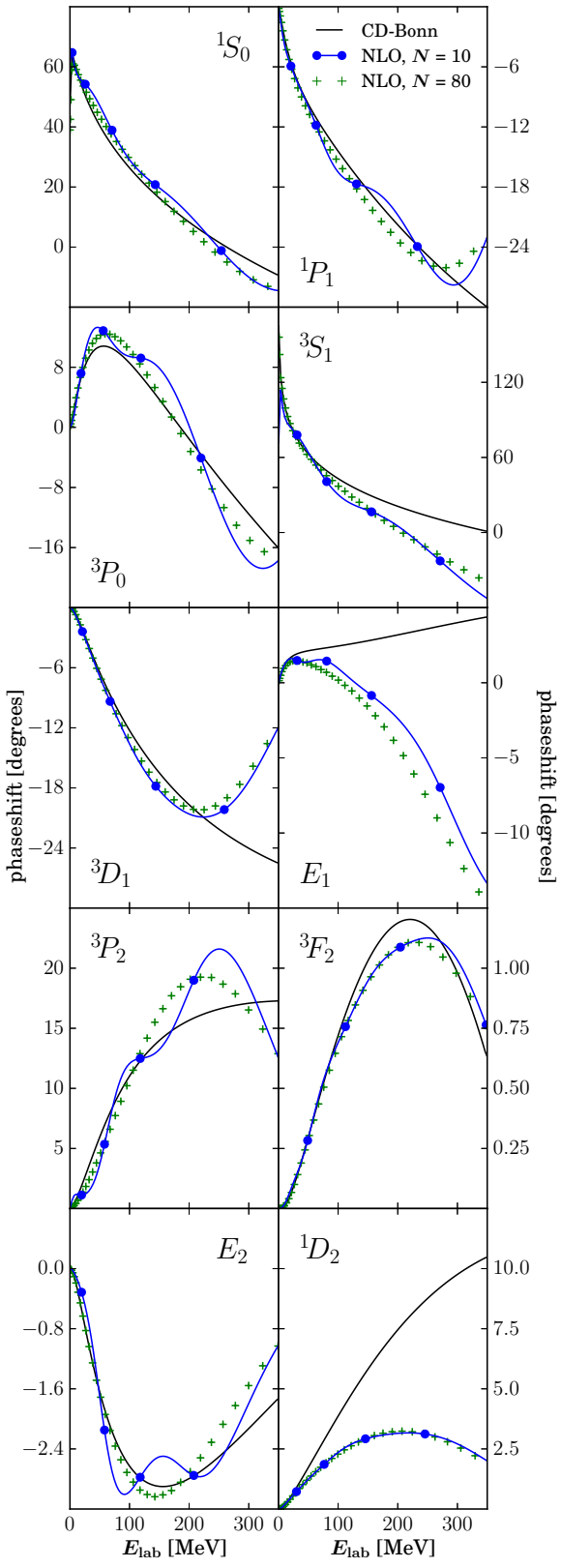

FIG. 5. (Color online) Phase shift from oscillator EFT at NLO with $N_{\max}=10$ (full blue circles and blue line) compared to those of the CD Bonn interaction (full black line) for partial wave channels as indicated. The green crosses show results from a large model space with $N_{\max}=80$.

	$N_{\max}=10$	$N_{\max}=80$	experiment
E_d [MeV]	−2.227	2.221	−2.225
r_d [fm]	1.984	1.961	1.976
Q_d [fm^2]	0.229	0.259	0.286
P_d	0.026	0.028	
$\tilde{C}^{(np)}_{^1S_0}$	−0.140992	−0.139687	
$\tilde{C}^{(pp)}_{^1S_0}$	−0.13991	−0.13855	
$\tilde{C}^{(nn)}_{^1S_0}$	−0.14046	−0.13913	
$C_{^1S_0}$	1.2470	1.2601	
$\tilde{C}_{^3S_1}$	−0.1604	−0.1825	
$C_{^3S_1}$	−0.682	−0.361	
C_{E_1}	0.250	0.236	
$C_{^3P_0}$	1.1629	1.1896	
$C_{^1P_1}$	0.348	0.366	
$C_{^3P_1}$	−0.336	−0.320	
$C_{^3P_2}$	−0.1647	−0.1697	

TABLE III. Deuteron properties (as in Table I) and LECs from effective interactions in $N_{\max}=10$ and 80 shells obtained from a fit to CD-Bonn phase shifts and deuteron properties. The oscillator frequencies are $\hbar\omega = 24$ MeV and 4 MeV for $N_{\max}=10$ and 80, respectively.

$N^{\rm lab}$	^{4}He	^{16}O	^{40}Ca	^{90}Zr	^{132}Sn
	$E_{\rm CCSD}$ [MeV]				
10	-31.57	-142.89	-402.0	-918.4	-1230.0
12	-31.57	-142.92	-402.4	-923.1	-1249.3
14	-31.57	-142.93	-402.5	-924.6	-1255.6
16	-31.57	-142.93	-402.5	-925.1	-1258.3
∞	-31.57	-142.93	-402.5	-925.4	-1260.1
exp	-28.30	-127.62	-342.1	-783.9	-1102.9
	r^2 [fm^2]				
10	1.78	4.14	6.58	9.70	11.60
12	1.78	4.15	6.60	9.77	11.79
14	1.78	4.15	6.60	9.80	11.85
16	1.78	4.15	6.61	9.82	11.88
∞	1.78	4.15	6.61	9.83	11.89
exp	2.12	6.60	11.41	17.57	21.57

TABLE IV. Ground-state energies $E_{\rm CCSD}$ and squared point-proton radii r^2 for nuclei ranging from ^{4}He to ^{132}Sn from CCSD calculations in many-body model spaces built from single-particle oscillator bases with $N^{\rm lab}=10,\ldots,16$. In the relative frame the oscillator EFT interaction is defined in the $N_{\max}=10$ model space, and the Hamiltonian matrix elements outside this space are comprised of the kinetic energy only. Experimental data taken from [68, 69]. The experimental point-proton radii are extracted from charge radii by correcting for the finite sizes of the proton and neutron, and the Darwin-Foldy term.

$^1D_2$ channel is an obvious exception, as it deviates more clearly from the CD-Bonn phase shifts at higher energies, but we note that at NLO there is no LEC to adjust in this channel. For E_1, the deviations are also considerable, however, it is of NLO quality, see Fig. 4. For the deuteron, we obtain a good reproduction of the binding energy and radius, and a reasonably well result for the quadrupole moment, as shown in Table III. The LECs, also shown in Table III, are natural in size and similar to NLO$_{\rm sim}$; the largest deviation is for the LEC $C_{^1P_1}$ which is only about 1/3 of its NLO$_{\rm sim}$ counterpart.

We utilize the NLO interaction in coupled-cluster calculations at the singles and doubles level (CCSD) [21, 66, 67] of the nuclei ^{4}He, ^{16}O, ^{40}Ca, ^{90}Zr, and ^{132}Sn. The coupled-cluster calculations use Hartree-Fock bases that are unitarily equivalent to the oscillator bases but lead to improved results. In these calculations, we keep the oscillator spacing fixed at $\hbar\omega = 24$ MeV in the spirit of oscillator EFT. We employ model spaces from $N^{\rm lab}=10$ up to $N^{\rm lab}=16$. In the oscillator basis, the potential is always restricted to $N_{\max}=10$, while the kinetic energy is used in the entire model space. The results are shown in Table IV. The $N^{\rm lab}=16$ point is used to gauge convergence of the results. For the light nuclei, energies and radii are practically IR converged already for $N^{\rm lab}=10$ because $r^2 \ll L^2$.

The convergence with respect to $N^{\rm lab}$ is very fast compared to other interactions from chiral EFT with a cutoff of around $\Lambda_\chi \approx 450$ MeV [6]. For IR extrapolations of ground-state energies E we employ [44]

$$E(L) = E_\infty + a e^{-2k_\infty L}, \tag{43}$$

where $L \approx \sqrt{2(N^{\rm lab}+7/2)}b$ is the IR length [45]. In the fit, we employ a theoretical uncertainty $\sigma \equiv \exp(-2k_\infty L)/(k_\infty L)$ to account for omitted corrections beyond the leading-order result (43). The difference between the IR extrapolated energies and the energy at $N^{\rm lab}=16$ is much smaller than both, the uncertainty of about 7% in correlation energy due to the CCSD approximation, and the uncertainty expected from higher orders in the chiral expansion.

Figure 6 (top) shows the result of an IR extrapolation for the ground-state energy of ^{132}Sn. Here, we plotted energies in $N^{\rm lab}=10$ to 16 as a function of the IR length L and also show the exponential IR extrapolation [44] The inset of Fig. 6 confirms the exponential convergence of the energy.

Figure 6 (bottom) shows the results of an IR extrapolation for the ground-state expectation value of the squared radius of ^{132}Sn. We plotted squared point-proton radii in model spaces with $N^{\rm lab}=10$ to 16 as a function of the IR length L and performed a χ^2 fit to the IR extrapolation [44]

$$r^2(L) = r^2_\infty - b(k_\infty L)^3 e^{-2k_\infty L}. \tag{44}$$

In the χ^2 fit of the radius, we refit the constant k_∞ and employed theoretical uncertainties $\sigma \equiv k_\infty L \exp(-2k_\infty L)$ to account for corrections to the leading-order result (44). Numerical results for the radii are listed in Table IV. The results from IR extrapolations involving only the data points from $N^{\rm lab}=10$ to 14 yield $E_\infty = -1259.2$ MeV and $r^2_\infty = 11.88$ fm^2 for ^{132}Sn, which are close to the previous results including the $N^{\rm lab}=16$ points.

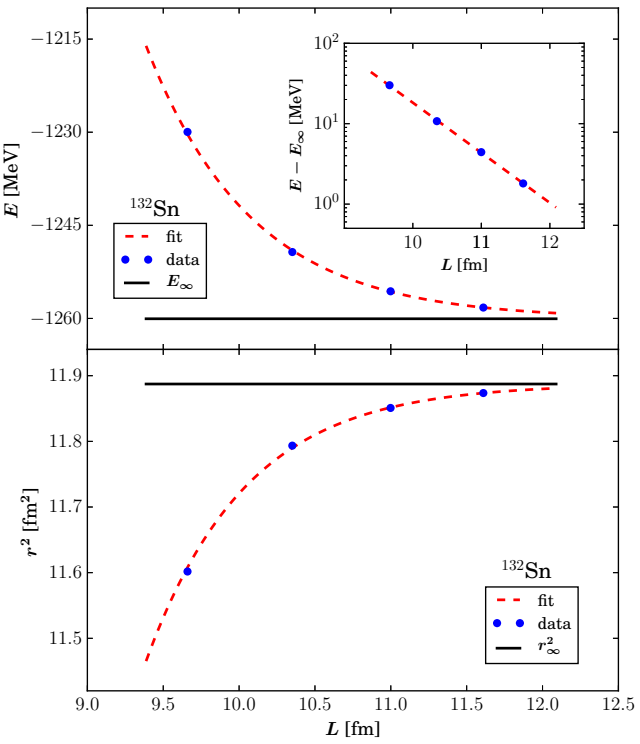

FIG. 6. (Color online) IR convergence of the ground-state energy (top) and squared radius (bottom) of ^{132}Sn computed from CCSD calculations using the oscillator EFT interaction. Data is shown as blue points, the extrapolations as red dashed lines, and the asymptotic energy and radius as solid black lines. The inset on the top shows that the ground-state energy is approached exponentially in the IR length L.

The oscillator EFT interaction at NLO overbinds nuclei by about 1 MeV per nucleon, and radii are too small. We note that the difference between theoretical and experimental values for the ground-state energies seem to be consistent with expectations from an NLO interaction. We also note that three-nucleon forces entering at next-to-next-to-leading order will be part of the saturation mechanism [26, 70].

The rapid convergence of ground-state energies and radii in oscillator EFT suggests that chiral cutoffs of $\Lambda_\chi \approx 450$ MeV are reasonable in nuclear-structure computations of heavy nuclei. Similar to renormalization group transformations the oscillator EFT reduces the mismatch between the tail of the momentum-space regulator and the oscillator space.

V. SUMMARY

We developed an EFT directly in the oscillator basis. In this approach UV convergence is implemented by construction, and IR convergence can be achieved by enlarging the model space for the kinetic energy only. We discussed practical aspects of the oscillator EFT and gave analytical expressions for the efficient calculation of matrix elements in oscillator EFT from their continuous-momentum counterparts. Within the J-matrix approach we computed phase shifts while working exclusively in the oscillator basis. Our results suggest that oscillations in the phase shifts appear when the UV cutoff imposed by the oscillator basis cuts into the high-momentum tails of the chiral interaction. To validate the oscillator EFT approach we reproduced a chiral interaction at NLO. Finally, we developed a chiral NLO interaction in oscillator EFT by optimizing the LECs to CD-Bonn phase shifts and experimental deuteron data. Coupled-cluster calculations for nuclei from ^{4}He up to ^{132}Sn exhibit a rapid convergence for ground-state energies and radii. These results suggest that the oscillator EFT is a promising candidate to facilitate *ab initio* calculations of heavy atomic nuclei based on interactions from chiral EFT using currently available many-body methods.

ACKNOWLEDGMENTS

We are grateful to R. J. Furnstahl and S. König for helpful discussions and comments on the manuscript. We also thank J. Rotureau for helpful discussions. This material is based upon work supported in part by the U.S. Department of Energy, Office of Science, Office of Nuclear Physics, under Award Numbers DE-FG02-96ER40963 (University of Tennessee), DE-SC0008499 (SciDAC-3 NUCLEI Collaboration), the Field Work Proposal ERKBP57 at Oak Ridge National Laboratory (ORNL), and under contract number DEAC05-00OR22725 (ORNL). S.B. gratefully acknowledges the financial support from the Alexander-von-Humboldt Foundation (Feodor-Lynen fellowship).

Appendix: Matrix elements in oscillator EFT

In this Appendix we give an alternative motivation for the computation (29) of matrix elements in oscillator EFT. These results are well known for DVRs, see, e.g., Ref. [55]. The projection onto a finite oscillator space is based on the usual scalar product

$$\langle\tilde{\Psi}_f|\tilde{\Psi}_g\rangle = \int_0^\infty \mathrm{d}k k^2 \tilde{\Psi}_f(k)\tilde{\Psi}_g(k) \qquad \text{(A.1)}$$

for radial wave functions in momentum space. The projection operator onto the finite oscillator space at fixed angular momentum l is

$$\hat{\Pi}_l \equiv \sum_{\nu=0}^{N} |\phi_{\nu,l}\rangle\langle\phi_{\nu,l}|. \qquad \text{(A.2)}$$

Let us alternatively consider a different projection operator, which is based on a different scalar product. We

write momentum-space wave functions with angular momentum l as

$$\tilde{\Psi}_f(k) = \sqrt{2b^3}(kb)^l e^{-\frac{1}{2}(kb)^2} f(k^2b^2). \tag{A.3}$$

Here, $f(x)$ is a polynomial in $x = k^2b^2$. It is clear that any square-integrable wave function can be built from such polynomials (with Laguerre polynomials $L_n^{l+1/2}$ being an example). We define the (semi-definite) scalar product $(\cdot|\cdot)$ of two functions $\tilde{\Psi}_f$ and $\tilde{\Psi}_g$ as

$$(\tilde{\Psi}_f|\tilde{\Psi}_g) \equiv \sum_{\mu=0}^{N} w_{\mu,l} f(x_{\mu,l}) g(x_{\mu,l}). \tag{A.4}$$

Here, the weights are from Eq. (21) and the abscissas $x_{\mu,l} \equiv k_{\mu,l}^2 b^2$ are the zeros of the associated Laguerre polynomial $L_{N+1}^{l+1/2}$ as demanded by $(N+1)$-point Gauss-Laguerre quadrature. Equation (A.4) defines only a semi-definite inner product, because $(\tilde{\Psi}_f|\tilde{\Psi}_f) = 0$ for any polynomial f with $f(x_{\mu,l}) = 0$ for $\mu = 0, \ldots, N$.

Several comments are in order. First, this semi-definite scalar product is identical to the standard scalar product (A.1) for wave functions $\tilde{\Psi}_f(k)$ that are limited to the finite oscillator space. To see this, we note that

$$\begin{aligned}\langle\tilde{\Psi}_f|\tilde{\Psi}_g\rangle &= \int_0^\infty \mathrm{d}k k^2 \tilde{\Psi}_f(k)\tilde{\Psi}_g(k) \\ &= \int_0^\infty \mathrm{d}x x^{l+1/2} e^{-x} f(x) g(x) \\ &= \sum_{\mu=0}^{N} w_{\mu,l} f(x_{\mu,l}) g(x_{\mu,l}).\end{aligned} \tag{A.5}$$

Here, we introduced the dimensionless integration variable $x \equiv k^2b^2$ in the second line and employ $(N+1)$-point Gauss-Laguerre quadrature in the third line. We note that $(N+1)$-point Gauss-Laguerre quadrature is exact for polynomials of degree up to and including $2N+1$, i.e., it is exact for polynomials f, g spanned by $L_n^{l+1/2}(x)$ with $n = 0, \ldots, N$.

This implies that the basis functions $\tilde{\psi}_{n,l}(k)$ with $n = 0, \ldots, N$ in the finite oscillator space remain a basis under the semi-definite scalar product, i.e.

$$(\tilde{\psi}_{n,l}|\tilde{\psi}_{n',l}) = \delta_n^{n'}. \tag{A.6}$$

Second, we note that both scalar products also agree for $N \to \infty$ because Gauss-Laguerre integration becomes exact in this limit.

Rewriting the weights $w_{\nu,l}$ in Eq. (21) as

$$\begin{aligned}w_{\nu,l} &= \frac{2b^3(k_{\nu,l}b)^2(k_{\nu,l}b)^{2l}e^{-(k_{\nu,l}^2b^2)}}{(N+1)(N+l+3/2)\left[\tilde{\psi}_{N,l}(k_{\nu,l})\right]^2} \\ &= 2b^3(k_{\nu,l}b)^l e^{-\frac{1}{2}(k_{\nu,l}^2b^2)} c_{\nu,l}^2,\end{aligned} \tag{A.7}$$

and using Eq. (13) yields another useful expression for the scalar product (A.4)

$$(\tilde{\Psi}_f|\tilde{\Psi}_g) = \sum_{\mu=0}^{N} c_{\mu,l}^2 \tilde{\Psi}_f(k_{\mu,l})\tilde{\Psi}_g(k_{\mu,l}). \tag{A.8}$$

A main difference between the scalar products of Eq. (A.1) and Eq. (A.8) arises when one compares the wave function

$$\langle k, l|\phi_{\nu,l}\rangle = \tilde{\phi}_{\nu,l}(k) \tag{A.9}$$

of Eq. (15) with the corresponding scalar product

$$\begin{aligned}(k, l|\tilde{\phi}_{\nu,l}) &= \sum_{\mu=0}^{N} c_{\mu,l}^2 \frac{\delta(k-k_{\mu,l})}{k^2} \tilde{\phi}_{\nu,l}(k_{\nu,l}) \\ &= c_{\nu,l}\frac{\delta(k-k_{\nu,l})}{k_{\nu,l}^2}.\end{aligned} \tag{A.10}$$

Here, we used Eq. (A.8) and Eq. (15) implying $\tilde{\phi}_{\mu,l}(k_{\lambda,l}) = c_{\lambda,l}^{-1}\delta_\mu^\lambda$. Clearly, the Fourier-Bessel transform (15) of the discrete momentum eigenstate $\phi_{\nu,l}$ has a complicated momentum dependence, while $(k, l|\tilde{\phi}_{\nu,l})$ is simply a rescaled δ function. This simple view is consistent with naive expectation of a momentum eigenstate.

We are now in the position to compute matrix elements based on the inner product (A.4). We note that

$$\begin{aligned}\hat{V}|\phi_{\mu,l}\rangle &= \hat{V}\int_0^\infty \mathrm{d}k k^2 |k, l\rangle(k, l|\phi_{\mu,l}) \\ &= \hat{V}|k_{\mu,l}\rangle c_{\mu,l}.\end{aligned} \tag{A.11}$$

Here, we used Eq. (A.10). Repeating the procedure on the bra side yields

$$(\phi_{\nu,l'}|\hat{V}|\phi_{\mu,l}) = \langle k_{\nu,l'}, l'|\hat{V}|k_{\mu,l}, l\rangle c_{\nu,l'}c_{\mu,l}, \tag{A.12}$$

and this is Eq. (29). We repeat that this derivation of the interaction matrix element is based on the scalar product (A.8) and not on the usual scalar product (A.1) for square integrable functions. We argue that the former scalar product is more natural considering the discrete momentum mesh that is employed in oscillator EFT.

For another view on the semi-definite scalar product we consider the projection operator

$$\hat{P}_l \equiv \sum_{n=0}^{N} |\tilde{\psi}_{n,l})(\tilde{\psi}_{n,l}|. \tag{A.13}$$

Indeed, $\hat{P}_l^2 = \hat{P}_l$. This makes it interesting to consider the projected wave function

$$\begin{aligned}\left(\hat{P}_l\tilde{\Psi}_f\right)(k_{\mu,l}) &= \sum_{n=0}^{N}(\tilde{\psi}_{n,l}|\tilde{\Psi}_f)\tilde{\psi}_{n,l}(k_{\mu,l}) \\ &= \sum_{\nu=0}^{N} c_{\nu,l}^2 \tilde{\Psi}_f(k_{\nu,l}) \sum_{n=0}^{N} \tilde{\psi}_{n,l}(k_{\nu,l})\tilde{\psi}_{n,l}(k_{\mu,l}) \\ &= \tilde{\Psi}_f(k_{\mu,l}).\end{aligned} \tag{A.14}$$

Here, we evaluated the sum over n using Eq. (17) when going from the second to the third line. Equation (A.14) shows that the projected wave function agrees with the full wave function at the discrete momenta $k_{\mu,l}$. In other words, the projection based on the semi-definite scalar product yields wave functions in finite oscillator spaces that agree with the unprojected wave functions at the physical momenta.

Let us give another interpretation of the projection $\hat{P}_l$. One finds for the scalar product (A.8)

$$(\tilde{\Psi}_f|\tilde{\Psi}_g) = \sum_{\mu=0}^{N} c_{\mu,l}^2 \tilde{\Psi}_f(k_{\mu,l})\tilde{\Psi}_g(k_{\mu,l}) = \langle\tilde{\Psi}_f| \left(\sum_{\mu=0}^{N} |k_{\mu,l},l\rangle c_{\mu,l}^2 \langle k_{\mu,l},l| \right) |\tilde{\Psi}_g\rangle. \quad \text{(A.15)}$$

Thus, the scalar product $(\tilde{\Psi}_f|\tilde{\Psi}_g)$ can be viewed as a matrix element of the operator in the brackets.

[1] E. Epelbaum, H.-W. Hammer, and Ulf-G. Meißner, "Modern theory of nuclear forces," Rev. Mod. Phys. **81**, 1773–1825 (2009).

[2] R. Machleidt and D.R. Entem, "Chiral effective field theory and nuclear forces," Physics Reports **503**, 1 – 75 (2011).

[3] P. Maris, J. P. Vary, and A. M. Shirokov, "*Ab initio* no-core full configuration calculations of light nuclei," Phys. Rev. C **79**, 014308 (2009).

[4] G. Hagen, T. Papenbrock, D. J. Dean, and M. Hjorth-Jensen, "*Ab initio* coupled-cluster approach to nuclear structure with modern nucleon-nucleon interactions," Phys. Rev. C **82**, 034330 (2010).

[5] E. D. Jurgenson, P. Maris, R. J. Furnstahl, P. Navrátil, W. E. Ormand, and J. P. Vary, "Structure of p-shell nuclei using three-nucleon interactions evolved with the similarity renormalization group," Phys. Rev. C **87**, 054312 (2013).

[6] Robert Roth, Angelo Calci, Joachim Langhammer, and Sven Binder, "Evolved chiral $nn+3n$ hamiltonians for *ab initio* nuclear structure calculations," Phys. Rev. C **90**, 024325 (2014).

[7] S. K. Bogner, T. T. S. Kuo, and A. Schwenk, "Model-independent low momentum nucleon interaction from phase shift equivalence," Physics Reports **386**, 1 – 27 (2003).

[8] S. K. Bogner, R. J. Furnstahl, and R. J. Perry, "Similarity renormalization group for nucleon-nucleon interactions," Phys. Rev. C **75**, 061001 (2007).

[9] E. D. Jurgenson, P. Navrátil, and R. J. Furnstahl, "Evolution of nuclear many-body forces with the similarity renormalization group," Phys. Rev. Lett. **103**, 082501 (2009).

[10] A. F. Lisetskiy, M. K. G. Kruse, B. R. Barrett, P. Navratil, I. Stetcu, and J. P. Vary, "Effective operators from exact many-body renormalization," Phys. Rev. C **80**, 024315 (2009).

[11] Micah D. Schuster, Sofia Quaglioni, Calvin W. Johnson, Eric D. Jurgenson, and Petr Navrátil, "Operator evolution for *ab initio* theory of light nuclei," Phys. Rev. C **90**, 011301 (2014).

[12] Dean Lee, "Lattice simulations for few- and many-body systems," Progress in Particle and Nuclear Physics **63**, 117 – 154 (2009).

[13] M. Lüscher, "Volume Dependence of the Energy Spectrum in Massive Quantum Field Theories. 1. Stable Particle States," Commun. Math. Phys. **104**, 177 (1986).

[14] Petr Navrátil, Sofia Quaglioni, Ionel Stetcu, and Bruce R Barrett, "Recent developments in no-core shell-model calculations," Journal of Physics G: Nuclear and Particle Physics **36**, 083101 (2009).

[15] Bruce R. Barrett, Petr Navrátil, and James P. Vary, "Ab initio no core shell model," Progress in Particle and Nuclear Physics **69**, 131 – 181 (2013).

[16] G. Hagen, M. Hjorth-Jensen, G. R. Jansen, R. Machleidt, and T. Papenbrock, "Evolution of shell structure in neutron-rich calcium isotopes," Phys. Rev. Lett. **109**, 032502 (2012).

[17] Jason D. Holt, Takaharu Otsuka, Achim Schwenk, and Toshio Suzuki, "Three-body forces and shell structure in calcium isotopes," Journal of Physics G: Nuclear and Particle Physics **39**, 085111 (2012).

[18] F. Wienholtz, D. Beck, K. Blaum, Ch. Borgmann, M. Breitenfeldt, R. B. Cakirli, S. George, F. Herfurth, J. D. Holt, M. Kowalska, S. Kreim, D. Lunney, V. Manea, J. Menendez, D. Neidherr, M. Rosenbusch, L. Schweikhard, A. Schwenk, J. Simonis, J. Stanja, R. N. Wolf, and K. Zuber, "Masses of exotic calcium isotopes pin down nuclear forces," Nature **498**, 346–349 (2013).

[19] V. Somà, A. Cipollone, C. Barbieri, P. Navrátil, and T. Duguet, "Chiral two- and three-nucleon forces along medium-mass isotope chains," Phys. Rev. C **89**, 061301 (2014).

[20] T. A. Lähde, E. Epelbaum, H. Krebs, D. Lee, U.-G. Meißner, and G. Rupak, "Lattice effective field theory for medium-mass nuclei," Phys. Lett. B **732**, 110 – 115 (2014).

[21] G. Hagen, T. Papenbrock, M. Hjorth-Jensen, and D. J. Dean, "Coupled-cluster computations of atomic nuclei," Reports on Progress in Physics **77**, 096302 (2014).

[22] H. Hergert, S. K. Bogner, T. D. Morris, S. Binder, A. Calci, J. Langhammer, and R. Roth, "*Ab initio* multireference in-medium similarity renormalization group calculations of even calcium and nickel isotopes," Phys. Rev. C **90**, 041302 (2014).

[23] G. Hagen, A. Ekström, C. Forssén, G. R. Jansen, W. Nazarewicz, T. Papenbrock, K. A. Wendt, S. Bacca, N. Barnea, B. Carlsson, C. Drischler, K. Hebeler, M. Hjorth-Jensen, M. Miorelli, G. Orlandini, A. Schwenk, and J. Simonis, "Neutron and weak-charge distributions of the ^{48}Ca nucleus," Nature Physics **12**, 186 (2016).

[24] Sven Binder, Joachim Langhammer, Angelo Calci, and Robert Roth, "Ab initio path to heavy nuclei," Physics Letters B **736**, 119 – 123 (2014).

[25] A. Ekström, G. Baardsen, C. Forssén, G. Hagen, M. Hjorth-Jensen, G. R. Jansen, R. Machleidt,

W. Nazarewicz, T. Papenbrock, J. Sarich, and S. M. Wild, "Optimized chiral nucleon-nucleon interaction at next-to-next-to-leading order," Phys. Rev. Lett. **110**, 192502 (2013).
[26] A. Ekström, G. R. Jansen, K. A. Wendt, G. Hagen, T. Papenbrock, B. D. Carlsson, C. Forssén, M. Hjorth-Jensen, P. Navrátil, and W. Nazarewicz, "Accurate nuclear radii and binding energies from a chiral interaction," Phys. Rev. C **91**, 051301 (2015).
[27] B. D. Carlsson, A. Ekström, C. Forssén, D. Fahlin Strömberg, G. R. Jansen, O. Lilja, M. Lindby, B. A. Mattsson, and K. A. Wendt, "Uncertainty analysis and order-by-order optimization of chiral nuclear interactions," Phys. Rev. X **6**, 011019 (2016).
[28] D. R. Entem, N. Kaiser, R. Machleidt, and Y. Nosyk, "Peripheral nucleon-nucleon scattering at fifth order of chiral perturbation theory," Phys. Rev. C **91**, 014002 (2015).
[29] E. Epelbaum, H. Krebs, and U.-G. Meißner, "Precision nucleon-nucleon potential at fifth order in the chiral expansion," Phys. Rev. Lett. **115**, 122301 (2015).
[30] A. Gezerlis, I. Tews, E. Epelbaum, M. Freunek, S. Gandolfi, K. Hebeler, A. Nogga, and A. Schwenk, "Local chiral effective field theory interactions and quantum monte carlo applications," Phys. Rev. C **90**, 054323 (2014).
[31] W. C. Haxton and C.-L. Song, "Morphing the shell model into an effective theory," Phys. Rev. Lett. **84**, 5484–5487 (2000).
[32] W. C. Haxton and T. Luu, "Perturbative effective theory in an oscillator basis?" Phys. Rev. Lett. **89**, 182503 (2002).
[33] W. C. Haxton, "Harmonic-oscillator-based effective theory," in *Opportunities with Exotic Beams* (World Scientific, 2007) Chap. 13, pp. 117–131.
[34] W. C. Haxton, "Form of the effective interaction in harmonic-oscillator-based effective theory," Phys. Rev. C **77**, 034005 (2008).
[35] I. Stetcu, B.R. Barrett, and U. van Kolck, "No-core shell model in an effective-field-theory framework," Physics Letters B **653**, 358 – 362 (2007).
[36] I. Stetcu, J. Rotureau, B. R. Barrett, and U. van Kolck, "Effective interactions for light nuclei: an effective (field theory) approach," Journal of Physics G: Nuclear and Particle Physics **37**, 064033 (2010).
[37] J. Rotureau, I. Stetcu, B. R. Barrett, and U. van Kolck, "Two and three nucleons in a trap, and the continuum limit," Phys. Rev. C **85**, 034003 (2012).
[38] J. Rotureau, I. Stetcu, B. R. Barrett, M. C. Birse, and U. van Kolck, "Three and four harmonically trapped particles in an effective-field-theory framework," Phys. Rev. A **82**, 032711 (2010).
[39] S. Tölle, H.-W. Hammer, and B. Ch. Metsch, "Universal few-body physics in a harmonic trap," Comptes Rendus Physique **12**, 59 – 70 (2011).
[40] S. Tölle, H.-W. Hammer, and B. Ch. Metsch, "Convergence properties of the effective theory for trapped bosons," Journal of Physics G: Nuclear and Particle Physics **40**, 055004 (2013).
[41] Eric J. Heller and Hashim A. Yamani, "New L^2 approach to quantum scattering: Theory," Phys. Rev. A **9**, 1201–1208 (1974).
[42] A. M. Shirokov, A. I. Mazur, S. A. Zaytsev, J. P. Vary, and T. A. Weber, "Nucleon-nucleon interaction in the j-matrix inverse scattering approach and few-nucleon systems," Phys. Rev. C **70**, 044005 (2004).
[43] S. A. Coon, M. I. Avetian, M. K. G. Kruse, U. van Kolck, P. Maris, and J. P. Vary, "Convergence properties of *ab initio* calculations of light nuclei in a harmonic oscillator basis," Phys. Rev. C **86**, 054002 (2012).
[44] R. J. Furnstahl, G. Hagen, and T. Papenbrock, "Corrections to nuclear energies and radii in finite oscillator spaces," Phys. Rev. C **86**, 031301 (2012).
[45] S. N. More, A. Ekström, R. J. Furnstahl, G. Hagen, and T. Papenbrock, "Universal properties of infrared oscillator basis extrapolations," Phys. Rev. C **87**, 044326 (2013).
[46] R. J. Furnstahl, S. N. More, and T. Papenbrock, "Systematic expansion for infrared oscillator basis extrapolations," Phys. Rev. C **89**, 044301 (2014).
[47] S. König, S. K. Bogner, R. J. Furnstahl, S. N. More, and T. Papenbrock, "Ultraviolet extrapolations in finite oscillator bases," Phys. Rev. C **90**, 064007 (2014).
[48] R. J. Furnstahl, G. Hagen, T. Papenbrock, and K. A. Wendt, "Infrared extrapolations for atomic nuclei," Journal of Physics G: Nuclear and Particle Physics **42**, 034032 (2015).
[49] K. A. Wendt, C. Forssén, T. Papenbrock, and D. Sääf, "Infrared length scale and extrapolations for the no-core shell model," Phys. Rev. C **91**, 061301 (2015).
[50] A.M. Shirokov, J.P. Vary, A.I. Mazur, and T.A. Weber, "Realistic nuclear hamiltonian: Ab exitu approach," Physics Letters B **644**, 33 – 37 (2007).
[51] D. O. Harris, G. G. Engerholm, and W. D. Gwinn, "Calculation of matrix elements for one-dimensional quantum-mechanical problems and the application to anharmonic oscillators," J. Chem. Phys. **43**, 1515–1517 (1965).
[52] A. S. Dickinson and P. R. Certain, "Calculation of matrix elements for one-dimensional quantum-mechanical problems," J. Chem. Phys. **49**, 4209–4211 (1968).
[53] J. C. Light, I. P. Hamilton, and J. V. Lill, "Generalized discrete variable approximation in quantum mechanics," J. Chem. Phys. **82**, 1400–1409 (1985).
[54] D. Baye and P.-H. Heenen, "Generalised meshes for quantum mechanical problems," J. Physics A: Math. Gen. **19**, 2041 (1986).
[55] R. G. Littlejohn, M. Cargo, T. Carrington, K. A. Mitchell, and B. Poirier, "A general framework for discrete variable representation basis sets," J. Chem. Phys. **116**, 8691–8703 (2002).
[56] J. C. Light and T. Carrington, "Discrete-variable representations and their utilization," in *Adv. Chem. Phys.* (John Wiley & Sons, Inc., 2007) pp. 263–310.
[57] A. Bulgac and M. McNeil Forbes, "Use of the discrete variable representation basis in nuclear physics," Phys. Rev. C **87**, 051301 (2013).
[58] L. S. Gradshteyn and L. M. Ryzhik, *Tables of integrals, series, and products*, 6th ed. (Academic Press, San Diego, 2000).
[59] P. Concus, D. Cassatt, G. Jaehnig, and E. Melby, "Tables for the evaluation of $\int_0^\infty x^\beta e^{-x} f(x)dx$ by Gauss-Laguerre quadrature," Math. Comp. **17**, 245–256 (1963).
[60] D. R. Entem and R. Machleidt, "Accurate charge-dependent nucleon-nucleon potential at fourth order of chiral perturbation theory," Phys. Rev. C **68**, 041001 (2003).
[61] Thomas Luu, Martin J. Savage, Achim Schwenk, and James P. Vary, "Nucleon-nucleon scattering in a har-

monic potential," Phys. Rev. C **82**, 034003 (2010).
[62] D. Stump, J. Pumplin, R. Brock, D. Casey, J. Huston, J. Kalk, H. L. Lai, and W. K. Tung, "Uncertainties of predictions from parton distribution functions. i. the lagrange multiplier method," Phys. Rev. D **65**, 014012 (2001).
[63] R. J. Furnstahl, N. Klco, D. R. Phillips, and S. Wesolowski, "Quantifying truncation errors in effective field theory," Phys. Rev. C **92**, 024005 (2015).
[64] J. E. Lynn, I. Tews, J. Carlson, S. Gandolfi, A. Gezerlis, K. E. Schmidt, and A. Schwenk, "Chiral three-nucleon interactions in light nuclei, neutron-α scattering, and neutron matter," Phys. Rev. Lett. **116**, 062501 (2016).
[65] R. Machleidt, "High-precision, charge-dependent Bonn nucleon-nucleon potential," Phys. Rev. C **63**, 024001 (2001).
[66] H. Kümmel, K. H. Lührmann, and J. G. Zabolitzky, "Many-fermion theory in expS- (or coupled cluster) form," Physics Reports **36**, 1 – 63 (1978).
[67] I. Shavitt and R. J. Bartlett, *Many-body Methods in Chemistry and Physics* (Cambridge University Press, 2009).
[68] M. Wang, G. Audi, A.H. Wapstra, F.G. Kondev, M. MacCormick, X. Xu, and B. Pfeiffer, "The AME 2012 atomic mass evaluation," Chinese Physics C **36**, 1603 (2012).
[69] I. Angeli and K.P. Marinova, "Table of experimental nuclear ground state charge radii: An update," At. Data Nucl. Data Tables **99**, 69 – 95 (2013).
[70] K. Hebeler, S. K. Bogner, R. J. Furnstahl, A. Nogga, and A. Schwenk, "Improved nuclear matter calculations from chiral low-momentum interactions," Phys. Rev. C **83**, 031301 (2011).